Deriving a Compact Analytical Model for Camera Response Functions with Application to Chartless Radiometric Calibration

Zhenhua Qu[†][*], Ziqiang He[*] and Xiangui Kang[*]
[†] Research Institute of China Telecom Ltd., Guangzhou, China
Email: qzhua3@gmail.com
[*] Guangdong Key Lab of Information Security, Sun Yat-Sen University, Guangzhou, China
Email: isskxg@mail.sysu.edu.cn

***Abstract*—Radiometric calibration (RC) is an essential preprocessing step to correct the non-linearity of camera output images. The chartless RC is a novel RC approach that does not need a color checker to do the calibration and attracts intensive research interests. A challenging issue in the chartless RC is how to reveal the parameters of the camera response function (CRF) more effectively from limited camera images. In this work, we take a general strategy for this issue by deriving more compact parametric CRF models. Firstly, a novel exponential exponent gamma curve (EEGC) model is proposed as a more compact superset to characterize the functional space of CRF. Then the general criteria for monotonic EEGCs (MEEGC) are derived. Finally, the analytical solution to low-order MEEGCs (AMEEGC) is proposed to get some nice constraint-free low-order analytical CRF models. The curve fitting experiments showed that the proposed models gave a more compact representation for real-world CRFs when compared to some existing models. We also demonstrated how to improve the efficiency of chartless RC algorithms with the 2nd-AMEEGC model by revisiting Takamatsu's noise-based method, and the results proved our method's superiority.**

I. Introduction

Camera response function(CRF) is a fundamental concept in digital imaging and computer vision. It resembles a non-linear relationship between the brightness of incident light and the output image pixel intensity. It is originated from the sensory non-linearity and/or the non-linear image enhancements and is depreciated in many vision-based tasks. For example, in panorama creation [1, 2], stereo reconstruction [3], autopilot and visual simultaneous localization and mapping(VSLAM) [4, 5], they would interfere the stereo matching processes and cause the systems to be less accurate. Thus an essential step in these tasks is to calibrate and restore the CRF non-linearity beforehand, which is often referred to as the "radiometric calibration(RC)." Traditionally, the RC experiments need to be conducted in a laboratory environment with a Macbeth color chart/checker [6] – a colored chessboard with patches of known reflectances. However, with the prevalence of consumer digital cameras and photo-taking cell phones, this precondition is usually not met. Moreover, with the rapid advancement of intelligent imaging technologies, many modern cameras can change their CRF adaptively according to the dynamic scene. And thus, the calibration results obtained in the laboratory may be inconsistent with those obtained in the field. In these circumstances, one might need the help of chartless RC methods, especially when it is inconvenient to carry the color charts in the wild.

The chartless RC problems have attracted intensive research interest recently. Researchers proposed a variety of chartless RC methods, *e.g.*, based on multiple images of different exposures [7, 8, 9], edge colors [10], geometry invariants [11], noise characteristics [12, 13, 14], motion blur [15, 16, 17, 18, 19], camera motion [20] or homography [1, 2, 21], skin pigment [22], and also deep learning [23]. A core issue of these problems is how to reveal the CRF more efficiently from limited camera output images. A universal strategy widely adopted is to employ a compact (low-order) representation of CRFs as to reduce the parameter space and accelerate the convergence during the optimization stage. Many low-order CRF models have been proposed, such as the generalized gamma curve (GGC) model proposed by Mann and Picard [24], the low-order polynomial model used by Mitsunaga and Nayar [8], the polynomial exponent gamma curve (PEGC) model proposed by Ng et al. [11], and also the pervasively used empirical model of response(EMoR) model proposed by Grossberg and Nayar [25]. However, a common issue is that they can not concisely characterize the functional space of CRFs, *e.g.*, some curves involved by them did not met the basic requirements of "valid" CRFs. One of the inconveniences brought by such redundancy is that we need to apply extra constraints while using these models, such as some forms of inequality constraints [25] or penalty terms on the monotone [16] or prior distribution [10] of the CRFs. These requirements would add to the burdens of the non-linear optimization process and make them harder to be solved.

In this work, we try to derive a more compact CRF model with other nice properties. To approach this goal, we shall delve into the mathematical basis for the CRFs. For the sake of brevity, the CRFs investigated here would be taken as global ones which work independently on each color channel. And a formal definition of the CRF's functional space is adopted

This work was supported by NSFC (Grant nos. 61772571, 62072484) and Chinese national key research and development project 2019QY2203.(Corresponding author: Xiangui Kang)

from Grossberg and Nayar [25].

*Definition 1 (**The Space of CRFs**):* The functional space of all valid CRFs, denoted by $\mathcal{W}_{CRF}$, can be given as follows:

$$\begin{aligned} O(x,y) \quad &= O_{\max} \cdot f\left(I(x,y)\right) + O_{\min},\ I(x,y) \in [0,1]\,, \\ s.t. \quad & f(0) = 0, \\ & f(1) = 1, \\ & f(\cdot) \text{ is monotonically increasing,} \end{aligned} \tag{1}$$

where $I(x,y)$ and $O(x,y)$ are the input light intensity and output pixel value at pixel location (x,y), respectively. For the CRFs here are location independent, the location (x,y) will be omitted in later formulations. $O_{\max}$ and $O_{\min}$ denote the largest and smallest pixel intensities for the output image. Without losing generality, one shall regard both the inputs and outputs as normalized, *i.e.*, $O_{\max} = 1$, $O_{\min} = 0$. And the CRF is reduced to $O = f(I)$. Correspondingly, the RC task can be considered as the process to recover I by reversely applying the CRFs, *i.e.*, $I = f^{-1}(O)$.

In seeking better representation for the CRFs' intrinsic properties, we summarized some of the practically appreciated properties of a CRF model from existing literature [1, 7, 8, 9, 13, 14], as follows:

*Definition 2 (**A "Good" CRF Model**):* A "good" CRF model should meet a plural of conditions,

1) **Across fixed points**: $f(0) = 0$, $f(1) = 1$.
2) **Monotonic**: Monotonically increasing within $[0,1]$.
3) **Bounded**: $0 \le f(I) \le 1$, $I \in [0,1]$.
4) **Smooth**: At least C^1 continuous(first-order differentiable).
5) **Extensible**: Gain accuracy by increasing parameters.
6) **Analytical**: Written in closed-form analytical terms without extra constraints.
7) **Compact**: Resemble typical real-world CRFs well with few parameters.

As can be expected, finding an ideal CRF model with all these virtues would be a non-trivial task. As to the best of our knowledge, none of the mentioned models had filled all these requirements.

In this work, we approach this purpose in three steps. Firstly, a novel *exponential exponent gamma curve (EEGC)* model is proposed to confine the functional space of CRF. Then the general criteria for *monotonic EEGC (MEEGC)* are derived. Finally, the *analytical solution to low-order MEEGC (AMEEGC)* is proposed to get a nice constraint-free low-order analytical CRF model– the 2nd-AMEEGC model. When compared with existing models, our model inherently conforms to all requirements in Definition 2 including good compactness and no need for explicit constraints.

The contributions of this work are as follows:

1) We proposed the EEGC/MEEGC models for the compact analytical modeling of CRFs. And the 2nd-AMEEGC is found to be an effective low-order analytical representation for typical CRFs.

2) With extensive curve fitting experiments, we showed that the compactness of the analytical MEEGC and 2nd-AMEEGC are superior than the existing analytical CRF models, and also comparable to the most compact numerical empirical CRF models, *i.e.*, the EMoR/logEMoR.

3) We applied the 2nd-AMEEGC to Takamatsu's noise-based chartless RC scenario. The experimental results demonstrated its superior performance in improving the convergence speed and also avoiding infeasible solutions.

The rest of the paper is organized as follows: In the next section, we first reviewed some existing works on CRF modeling in chartless RC. Then we derived a theoretical framework for CRFs involving the EEGC, the MEEGC, and the 2nd-AMEEGC in Section 3. In Sections 4 and 5, curve fitting experiments and a noise-based chartless RC task were used to validate the effectiveness of the proposed models. The concluding remarks are given in Section 6.

II. Related Works

A. CRF Modeling in Chartless RC

In the early days, chartless RC researchers focused on revealing the CRF from images of different exposures. Mann and Picard [24] firstly used a GGC model to simplify the CRF estimation. To address more complex CRFs, Debevec and Malik [7] formulated the problem with a high dimensional (256 dimensions) log domain non-parametric model with a smoothness constraint. Then Mitsunaga and Nayar [8] proposed the low-order polynomial(Poly) model and also the constrained polynomial(ConPoly) model which implicitly engaged the constraints of crossing $(0,0)$ and $(1,1)$. And later, Grossberg and Nayar [25] further improved the CRF model compactness with the principal component analysis (PCA)-based EMoR and logEMoR models. Recently, Grundmann et al. [26] proposed a linear mixture of EMoR models to represent more complex CRFs involved in video sequences. In these scenarios, the chartless RC problem was often given a quadratic programming(QP) framework, and thus even high dimensional CRF models could still be solved very efficiently. However, a fundamental issue of the different exposure based approach is that when the exposure ratios of the given images are identical or unknown, there will be a gamma fuzziness between the revealed CRF $\hat{f}(I)$ and the ground truth one, *i.e.*, $\hat{f}(I) = [f(I)]^{\gamma}$, which is known as the "Gamma/Exponential Ambiguity" [1, 7, 8, 26]. In consequence, the image non-linearity cannot be removed completely by applying $\hat{f}^{-1}(O)$.

Meanwhile, some researchers tried to explore other types of features to circumvent this obstacle. Some notable features involved the image noise [12, 13, 14], color linearity at object edges [10], locally planer [11, 27] or blurred areas [15, 17, 18, 19]. More recently, the skin pigment [22] and convolutional neural networks(CNN) based features [23] were also explored. Unfortunately, most of these attempts could not found a fast solution like the QP, and some general non-linear optimization frameworks had to be used. In these circumstances, a compact representation of CRF would be highly appreciated. Ng et al. [11] proposed a PEGC model, which merited in both good extensibility and compactness for representing CRFs. A defect of PEGC is that it grows exponentially and is unbounded which might cause numerical issues during the optimization. More researchers chose to use the EMoR/logEMoR model with additional inequality constraints or penalty terms [1, 10, 26, 28, 29]. However, these measures would somehow complicate the optimization procedures by introducing more tunable hyperparameters and compatibility issues, *e.g*., some nonlinear optimization algorithms do not accept inequality constraints, such as the *fminsearch* and *fminunc* in Matlab.

To summarize, let us remark that, to the best of our knowledge, none of these models had fully filled the rules of Definition 2 in Section I, *e.g*., the GGC model [24] does not consider the extensibility, the log-domain nonparametric model [7] is universal but highly redundant, Poly, ConPoly [8] and PEGC [11] is analytical but unbounded and not compact enough, the EMoR model [25] is highly compact but subject to numerical inequality constraints and empirical data. A fundamental question that needs to be asked is whether it is possible to found a "perfect" CRF model which could satisfy all the rules in Definition 2.

B. Takamatsu's Noise-Based Charless RC Method

In this work, we would demonstrate the effectiveness of the proposed models with a noise-based chartless RC scenario investigated by Takamatsu and Matsushita [14]. They revealed the CRF from noisy images taken from a static scene with identical exposure settings. The major defects of their method involved the intensive computation and also the common defects of most non-linear optimization problems, such as the risk of being slow convergence and stuck by infeasible solutions. Nevertheless, for their method has a constant computation cost which is independent to image contents, it would be more convenient to validate the efficiency improvement with the proposed compact CRF models in this scenario.

To set off, we shall briefly introduce the major steps of Takamatsu's method [14].

1) Firstly, they took multiple pictures from a static scene with identical exposure settings, *e.g*., exposure time, ISO, aperture, white balancing, etc.

2) Then a co-occurrence matrix $C(O_1, O_2)$ was accumulated from pixels at the same locations. O_i is the pixel intensity from the i'th observed output images.

3) Finally, they proposed an *Image Similarity Metric(ISM)* based cost function and adopted an expectation-maximization(EM)-like optimization strategy to reveal the CRF parameter and noise parameter alternatively. The detailed definition of the ISM-based cost function is as follows:

$$L(\boldsymbol{\alpha};\boldsymbol{\beta}) = \frac{1}{Z}\iint \frac{C(O_2,O_1)}{\sum_{O_2} C(O_2,O_1)} g'(O_2)\, S(g(O_1), g(O_2))\, dO_1 dO_2, \tag{2}$$

where the vector $\boldsymbol{\alpha}$ and $\boldsymbol{\beta}$ correspond to the CRF parameters and noise parameters, respectively. $g(O)$ is the ICRF. The $S(g(O_1), g(O_2))$ is the pixel-wise similarity metric defined in the input signal domain (raw sensor data of the camera)

$$S(I_1, I_2) = \int p\left(I_2|\tilde{I}\right) p\left(I_1|\tilde{I}\right) p\left(\tilde{I}\right) d\tilde{I}, \tag{3}$$

where $\tilde{I}$ is the noise-free ground truth input signal, while $I_1 = g(O_1)$ and $I_2 = g(O_2)$ are two noisy observations of $\tilde{I}$ revealed by the ICRF. The $p\left(I_i|\tilde{I}\right)$ is assumed to be a variable variance Gaussian distribution

$$p\left(I_i|\tilde{I}\right) = \mathcal{N}\left(\mu=\tilde{I}, \sigma^2=u\tilde{I}+v\right), \tag{4}$$

where $u \geq 0$ and $v \geq 0$ are the two parameters which constituted $\boldsymbol{\beta}$. Z is a normalization term defined as

$$Z = \sqrt{\iint S(I_1, I_2)^2 dI_1 dI_2}. \tag{5}$$

Overall, it is tough to improve the efficiency of this problem, for the intensive computation required by the numerical integration in Eq. (3) is solid. To handle this tricky problem, we would try out the proposed 2nd-AMEEGC model as to improve the efficiency of the optimization process. Detailed experimental results will be given in Section V.

III. A Compact Analytical Model for CRFs

In this section, we will derive a theoretical framework for the compact modeling of CRFs. Firstly, we will introduce a novel EEGC model for the general framework of CRF modeling. Then some closed-formed analytical solutions are derived for the low-order monotonic EEGCs.

A. The EEGC

The proposed EEGC is a generalization of the GGC[24] and PEGC [11] which can be defined as follows:

*Definition 3 (**The EEGC**):* The general form of EEGC is defined as:

$$f(I) = I^{\exp[\psi(I)]},\ I \in [0,1], \tag{6}$$

where $\psi(I)$ is defined as the kernel function of the EEGC. Without loss of generality, we focus on a polynomial kernel here

$$\psi(I) = \sum\nolimits_{j=0}^{N} \alpha_j I^j, \tag{7}$$

where the α_j's are the polynomial parameters. Then with an N'th order EEGC, we will have $N+1$ parameters in total. To be consistent, the order of other CRF models will also be expressed in this way.

The EEGC inherits many virtues from the GGC and PEGC [11], *e.g*., it goes across $(0,0)$, $(1,1)$ (rule 1), is highly differentiable (rule 4), can be written in analytical terms(rule 6) and reduces to a canonical gamma correction when $N=0$. Moreover, for its non-negative exponent, $f(I)$ will always be bounded within $[0,1]$ (rule 3). From the perspective of functional space, this boundness constraint makes the EEGC a more confined supper set for the space of CRFs. This would also lead to a mathematically induced compactness(rule 7), for a massive number of invalid functions have been eliminated. Meanwhile, with an extensible order, the EEGC can approximate arbitrary CRFs tightly within its hull (rule 5). When referring to the rules in in Definition 2, the only imperfection is that the monotonic constraint (rule 2) is not met. And we would address this issue in the next section.

B. The Monotonic EEGC

The EEGC model can be made more concise by eliminating those non-monotonic functions. In the past, this was usually achieved by explicitly engaging some constraints, *e.g.*, via inequalities constraints [25] and penalty terms on monotone [16] or prior distribution [10]. Nevertheless, in this section, we shall do this more implicitly by introducing some nice constraint-free low-order analytical CRF models.

1) The General Criteria for MEEGC: Firstly, we will derive the general criteria for the monotonic EEGC (MEEGC). The MEEGC can be obtained by simply reinforcing a monotonic constraint to EEGC, namely

$$f'(I) \geq 0, I \in (0,1). \tag{8}$$

With the polynomial kernel in Eq. (7) and some derivations, it turns out to be

$$\sum\nolimits_{j=1}^{N} j \cdot \alpha_j I^{j-1} \leq -1/\left(I \log I\right), I \in (0,1). \tag{9}$$

From a numerical point of view, this criteria can be turned into a linear inequality constraint

$$\mathbf{C}\boldsymbol{\alpha} \leq \mathbf{d} \tag{10}$$

where the vector $\boldsymbol{\alpha} = [\alpha_0, \alpha_1, \cdots, \alpha_N]^T$ corresponds to the parameters of MEEGC. The matrix $\mathbf{C}$ and vector $\mathbf{d}$ are defined as

$$\begin{aligned} C_{i,j} &= k\hat{I}_i^{j-1}, \\ d_i &= -1/\left(\hat{I}_i \log \hat{I}_i\right), \end{aligned} \tag{11}$$

where $\hat{I}_i = \frac{i}{M}$, $i = 1, ..., M-1$ are some discrete locations where the criteria are evaluated. And N and M resembles the model order and maximum number of sampled locations, respectively. And typically $M >= 256$.

Nevertheless, similar to the constraint involved in EMoR [30], it is hard to treat these boundary conditions for non-convex optimization problems. And also, many optimization algorithms used in chartless RC, *e.g.*, the *fminsearch* or *fminunc* in Matlab [14, 29], do not accept inequality constraints. In the next subsection, we would discuss how to get rid of them by deriving analytical solutions for MEEGCs.

2) The AMEEGCs: To avoid explicit constraints, we need to derive the analytical solution of MEEGC from Eq. (9). Although this would be intractable in a general sense, we found some explicit and approximate AMEEGC's for low-order MEEGCs ($ord < 3$).

i) ***The 0'th-AMEEGC***: It is a trivial case for AMEEGC. The 0'th MEEGC simply reduce to a gamma curve

$$\hat{f}_0\left(I\right) = I^{\exp(a)}, \tag{12}$$

where $a \in \mathbb{R}$ is the only parameter of the 0'th-AMEEGC.

ii) ***The 1st-AMEEGC***: The monotone is applied implicitly by re-writing the 1st-MEEGC into a constraint free form

$$\hat{f}_1\left(I\right) = I^{\exp\left[a + \left(e - b^2\right)I\right]}, \tag{13}$$

where $a, b \in \mathbb{R}$ are the two parameters of the 1st-AMEEGC. e is the natural constant.

iii) ***The 2nd-AMEEGC***: Analogously, the 2nd-AMEEGC could somehow be derived approximately as

$$\hat{f}_2\left(I\right) = I^{\exp\left[a + \left(e - b^2\right)I + \left(b^2 - \frac{c^2}{2}\right)I^2\right]}, \tag{14}$$

where a, b, $c \in \mathbb{R}$ are the three parameters of 2nd-AMEEGCs, and e is the natural constant.

An obvious advantage of these AMEEGCs over existing CRF models is that we can adjust their parameters arbitrarily without breaking the basic rules in Definition 2. In practice, we found the 2nd-AMEEGC to be a compact yet expressive representation for ordinary/typical CRFs, as will be addressed in Section IV.

IV. Experimental Validation

In this section, we conduct a curve fitting experiment to validate the compactness of the MEEGCs and AMEEGCs with real-world CRFs. The evaluation dataset is the Database of Response Functions(DoRF) [25]. As shown in Fig. 1, it contains 201 CRF curves which covered a wide range of photographic films, CCD/CMOS sensors, digital cameras, and some artificial gamma curves ($f(I) = I^{\gamma}, 0.2 < \gamma < 2.8$).

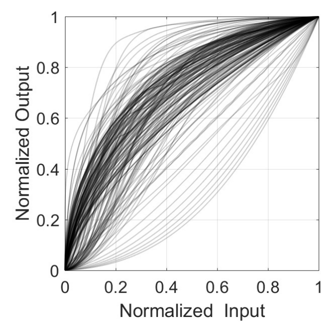

Fig. 1. The 201 CRFs from the DoRF dataset [25] used as the targets for the curve fitting experiments.

The performance of each curve fitting experiment is measured by the approximation error in terms of Root Mean Squared Error (RMSE)

$$\text{RMSE} = \sqrt{\frac{1}{N}\sum_{j=0}^{N-1}\left[O_j - f\left(I_j; \boldsymbol{\alpha}\right)\right]^2}, \tag{15}$$

where O_j and $f\left(I_j; \boldsymbol{\alpha}\right)$ are the ground truth and approximated CRF values at $I_j = j/N-1$, respectively. For DoRF, we use $N = 1024$. Empirically, an RMSE around 0.01 will be good enough for most chartless RC scenarios. And in non-ideal cases, the RMSEs would commonly reach up to 0.05. And the overall performance of a model can be judged by the distribution of the total RMSEs on DoRF.

Fig. 2 shows the variation of the curve fitting errors with the model order for each model. More compact models should have smaller errors at the same order. We can see the overall performances of MEEGCs and AMEEGCs are among the best regarding their error bars. Especially, at low-orders ($ord \leq 4$), the MEGGCs outperformed the EMoR and other existing analytical models. It also shows that the performance of the 2nd-AMEEGC is nearly identical to the numerically constrained 2nd-MEEGC.

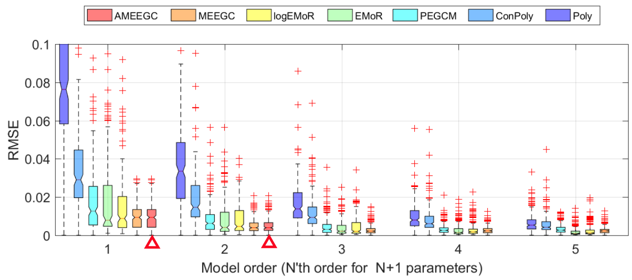

Fig. 2. Curve fitting performance comparison of the numerically constrained MEEGCs and the low-order analytical AMEEGCs in Eq. (14) to some existing models. The box plot shows the variation of the curve fitting errors with the model order for each model. In each error bar, the central mark indicates the median of the RMSEs obtained by fitting the 201 CRFs of the DoRF dataset [25]. The bottom and top edges indicate the 25th and 75th percentiles, and the outliers are marked with red "+." The red triangles marked the results of AMEEGCs which are only available up to the second order.

Fig. 3 gives some detailed examples for the curve fitting results of the 2nd-AMEEGC. We can see that in most cases, the 2nd-AMEEGC fitted the CRFs reasonably well (Fig. 3a). Meanwhile, it would have sightly larger approximation errors in a few cases when the CRF curves have large curvatures (Fig. 3b). Nevertheless, we need to address that such kinds of CRFs are not commonly seen in modern digital cameras [31], and also, a moderate approximation error is still tolerable in many applications.

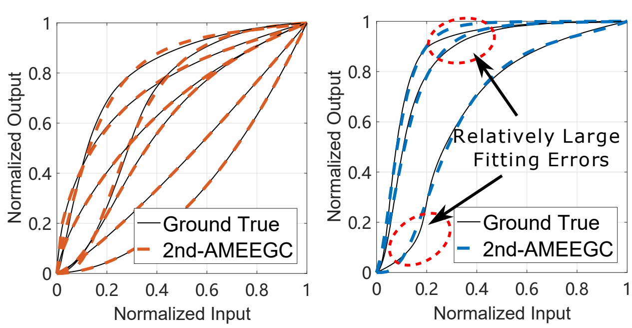

(a) (b)

Fig. 3. Some examples of the curve fitting results of the 2nd-AMEEGC. (a) gives some good approximation examples. (b) shows a few cases which have sightly larger approximation errors. In each subfigure, the solid lines are for the ground truth fitting target CRFs selected from the DoRF dataset [25]. And the dash lines are the corresponding CRFs reproduced from the 2nd-AMEEGC coefficients obtained by the curve fitting.

V. Applied to Chartless Radiometric Calibration

This section applies our 2nd-AMEEGC model to Takamatsu's noise-based chartless RC scenario [14] to demonstrate how to improve the method's efficiency by avoiding the risks of slow convergence and infeasible solutions. Detailed procedures of their method had been introduced in Section II-B. Here, we simply substituted the EMoR model with the proposed 2nd-AMEEGC and compare their performances in identical conditions. Detailed experimental configurations are as follows:

1) ***Data***: We generated some synthetic images to conduct a large-scale test. It would be appropriate here for our emphasis is the efficiency rather than the validity of Takamatsu's method [14]. The ground truth images were chosen from a collection of 20 scenery pictures (1600 $\times$ 900 pixels), as shown in Fig. 4. And a pair of corresponding noisy images were generated by adding random noise to the ground truth one. The noise parameters u and v of Eq. (4) were sampled randomly from uniform distributions $U(0.01, 0.06)$ and $U(9, 25)$, respectively. Finally, a tone mapping was applied with a CRF randomly picked from the 201 curves of the DoRF dataset [25]. For each ground truth, this process was repeated for ten times. So we generated 200 pairs of noisy synthetic pictures in total. Only the green channels of them were used for co-occurrence matrices extraction.

Fig. 4. The twenty scenery images of our synthetic image dataset.

2) ***Model***: Takamatsu's method [14] used the 4th-EMoR model without any further constraint nor regularization. In contrast, we will try the 2nd-AMEEGC out here. For both models, the raw coefficients have undergone a PCA pre-whitening step to reach the optimum convergence speed. For example, the whitened EMoR model would become:

$$\mathbf{g} = \mathbf{g}_0 + \mathbf{G}\boldsymbol{\Lambda}\mathbf{c}, \tag{16}$$

where the vector $\mathbf{g}$ is the numerical representation of the ICRF $g(O)$. The vector $\mathbf{c}$ resembles the coefficients of the whitened EMoR. $\mathbf{g}_0$ and $\mathbf{G} = [\mathbf{g}_1, \mathbf{g}_2, \cdots, \mathbf{g}_N]$ are the mean vector and the first N PCA eigenvectors obtained from the numerically inversed CRFs of DoRF. And the matrix $\boldsymbol{\Lambda}$ is a diagonal whitening matrix. Analogously, the whitened 2nd-AMEEGC coefficients can be obtained analogously with the curve fitting results in Section IV.

3) ***Optimization***: Takamatsu and Matsushita [14] suggested that the Nelder-Mead Simplex method [32](implemented by the *fminsearch* in Matlab) would be an effective optimization strategy for their problem. They also adopted an EM-like strategy to update the parameters of CRF and noise distribution alternatively. We followed these steps, and the total iteration

number of EM steps is set to 15. The maximum iteration number of *fminsearch* is set to 10. The initial parameters were fixed for both methods, *e.g*., the noise parameters were $u = 0.06$, $v = 1$, and the CRF parameters were corresponding to the identity mapping $f(I) = I$.

4) ***Environments***: The experiments were run on a PC server with an Intel 2.6GHz Xeon CPU(12 Cores) and 32GB of memory. And the GPU attached is the NVIDIA 1050Ti with 8GB of graphic memory. We implemented Takamatsu's algorithm with Matlab and accelerated the numerical integration part in Eq. (3) with the *gpuArray* functions.

5) ***Evaluation Criteria***: The performances of different models were measured from three aspects: 1) the overall convergence speed; 2) the occurrences of infeasible solutions;3) the overall CRF estimation error in terms of RMSE.

As shown in Fig. 5, the first row (subfigure a-c) gave the comparison of the 2nd-AMEEGC to the 4th-EMoR. We can see that the proposed 2nd-AMEEGC model not just converged faster (Fig. 5a), but also resulted in better CRF estimation accuracy in terms of RMSE distribution (Fig. 5c). These results illustrated that the compactness of the 2nd-AMEEGC brought efficiency without precision loss. Also, we noticed that in this scenario, both models did not have any infeasible solution, as shown in Fig. 5b.

Meanwhile, we also gave a comparison to the 2nd-EMoR in the second row of Fig. 5 (subfigure d-f) for a fair comparison. As shown in Fig. 5e, about 31% (62/200) of the cases in the 2nd-EMoR model test converged to infeasible solutions judging by their total variations. When they are ignored, as shown in Fig. 5d and Fig. 5f, it is fair to say the 2nd-EMoR has a similar convergence speed and estimation accuracy as the 2nd-AMEEGC. But when the re-trails for handling those infeasible cases were also considered, the actual converged speed for the 2nd-EMoR model would be much worse. These results revealed another advantage of the 2nd-AMEEGC, which is by conforming to all the rules in Definition 2, it is immune to the infeasible solutions.

Overall, these results have clearly shown that neither the high-order(4th order) EMoR nor the low-order(2nd order) one is comparable with the proposed 2nd-AMEEGC when used with Takamatsu's noise-based chartless RC method.

VI. Conclusions

In this work, we proposed a EEGC/MEEGC based framework to represent the functional space of CRFs more compactly. Then we showed how to impose implicit monotonic constraints on EEGC to obtain the 2nd-AMEEGC, which could compactly represent typical/ordinary CRFs. With all these efforts, we managed to show that it is possible to derive CRF models with many virtues: good compactness, extensible, analytical/closed-form and need no extra constraints to stand on their own. With the extensive experiments, the superior compactness of the proposed models was proven under the DoRF dataset. More specifically, we demonstrated how easily could the 2nd-AMEEGC be engaged to an existing chartless RC scenario to improve its performance. In the future, we hope to explore other possible applications of our method in the fields of computer vision, high dynamic imaging, and digital image forensics.

Acknowledgment

The authors would like to thank Dr. Beiling Lu and also the anonymous reviewers for their careful proof reading and valuable comments which have led to substantial improvements of this paper.

References

[1] S. J. Kim and M. Pollefeys, "Robust radiometric calibration and vignetting correction," *IEEE Trans. Pattern Anal. Mach. Intell.*, vol. 30, no. 4, pp. 562–576, Apr. 2008.
[2] D. B. Goldman, "Vignette and exposure calibration and compensation," *IEEE Trans. Pattern Anal. Mach. Intell.*, vol. 32, pp. 2276–2288, 2010.
[3] W. Mongkulmann, T. Okabe, and Y. Sato, "Photometric stereo with auto-radiometric calibration," in *Proc. IEEE Int. Conf. Computer Vision Workshops (ICCV Workshops)*, Nov. 2011, pp. 753–758.
[4] P. Bergmann, R. Wang, and D. Cremers, "Online photometric calibration of auto exposure video for realtime visual odometry and slam," *IEEE Robotics and Automation Letters*, vol. 3, pp. 627–634, 2018.
[5] P. Liu, X. Yuan, C. Zhang, Y. Song, C. Liu, and Z. Li, "Real-time photometric calibrated monocular direct visual slam," *Sensors (Basel, Switzerland)*, vol. 19, 2019.
[6] J. G. D. C. S. McCamy, H. Marcus, "A color rendition chart," *Journal of Photographic Engineering*, vol. 2, no. 3, 1976.
[7] P. E. Debevec and J. Malik, "Recovering high dynamic range radiance maps from photographs," in *Proc. of ACM SIGGRAPH*, 1997, pp. 369–378.
[8] T. Mitsunaga and S. Nayar, "Radiometric self calibration," in *Proc. of IEEE Conf. Computer Vision and Pattern Recognition(CVPR)*, vol. 1. Fort Collins, CO, USA: IEEE, 1999, pp. 374–380.
[9] M. D. Grossberg and S. K. Nayar, "Determining the camera response from images: What is knowable?" *IEEE Trans. Pattern Anal. Mach. Intell.*, vol. 25, pp. 1455–1467, 2003.
[10] S. Lin, J. Gu, S. Yamazaki, and H.-Y. Shum, "Radiometric calibration from a single image," in *Proc. of IEEE Conf. Computer Vision and Pattern Recognition(CVPR)*, vol. 2, 2004, pp. 938–945.
[11] T. T. Ng, S. F. Chang, and M. P. Tsui, "Using geometry invariants for camera response function estimation," in *Proc. of IEEE Conf. Computer Vision and Pattern Recognition(CVPR)*, Jun. 2007, pp. 1–8.
[12] Y. Tsin, V. Ramesh, and T. Kanade, "Statistical calibration of ccd imaging process," vol. 1, 2001, pp. 480–487.
[13] Y. Matsushita and S. Lin, "Radiometric calibration from noise distributions," in *Proc. of IEEE Conf. Computer Vision and Pattern Recognition(CVPR)*. Minneapolis, MN, USA: IEEE, 2007, pp. 1–8.
[14] J. Takamatsu and Y. Matsushita, "Estimating camera response functions using probabilistic intensity similarity," in *Proc. of IEEE Conf. Computer Vision and Pattern Recognition(CVPR)*, Jun. 2008, pp. 1–8.
[15] J. Y. Lee, B. Shi, Y. Matsushita, I. S. Kweon, and K. Ikeuchi, "Radiometric calibration by transform invariant low-rank structure," in *Proc. of IEEE Conf. Computer Vision and Pattern Recognition(CVPR)*, Jun. 2011, pp. 2337–2344.
[16] S. Kim, Y.-W. Tai, S. J. Kim, M. S. Brown, and Y. Matsushita, "Nonlinear camera response functions and image deblurring,"

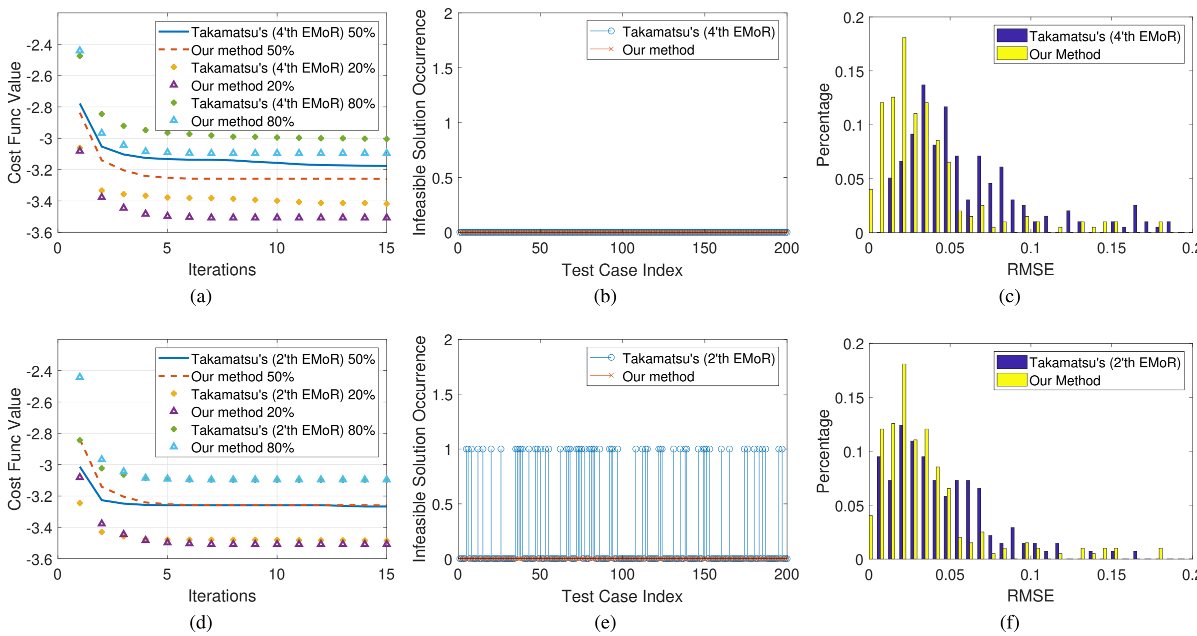

Fig. 5. Performance comparison with the proposed 2nd-AMEEGC and the EMoR model based on Takamatsu's method [14]. The first row and second raw are the comparisons to the 4th-EMoR and 2nd-EMoR, respectively. In each row, the first subfigure(left) gave the convergence speed comparison by plotting the 20%, 50%(median),80% percentiles of the cost function values(Eq. (2)) at each iteration of the optimization. The second subfigure (in the middle) gave the occurrences of infeasible solutions. Each stem indicates one occurrence of the infeasible solution. And the last subfigure (right) gave the RMSE distribution histograms of both methods. Higher bins near the zero point would be better. Note: for the 2nd-EMoR, the infeasible solutions are excluded from the calculation of convergence speed and the RMSE distribution, thus its actual performance could be worse.

in *Proc. of IEEE Conf. Computer Vision and Pattern Recognition(CVPR)*, 2012, pp. 25–32.

[17] J. Y. Lee, Y. Matsushita, B. Shi, I. S. Kweon, and K. Ikeuchi, "Radiometric calibration by rank minimization," *IEEE Trans. Pattern Anal. Mach. Intell.*, vol. 35, no. 1, pp. 144–156, Jan. 2013.

[18] Y. W. Tai, X. Chen, S. Kim, S. J. Kim, F. Li, J. Yang, J. Yu, Y. Matsushita, and M. S. Brown, "Nonlinear camera response functions and image deblurring: Theoretical analysis and practice," *IEEE Trans. Pattern Anal. Mach. Intell.*, vol. 35, no. 10, pp. 2498–2512, Oct. 2013.

[19] J. W. Huang, S. C. Liang, and H. Y. Lin, "A technique for deriving the camera response function using image blur," in *Proc. IEEE Int. Conf. Consumer Electronics - Taiwan*, Jun. 2015, pp. 338–339.

[20] R. Galego., A. Bernardino., and J. Gaspar., "Vignetting correction for pan-tilt surveillance cameras," in *Proc. of the Int. Conf. on Computer Vision Theory and Applications (VISAPP)*, INSTICC. SciTePress, 2011, pp. 638–644.

[21] A. Litvinov and Y. Schechner, "Radiometric framework for image mosaicking." *Journal of the Optical Society of America. A, Optics, image science, and vision*, vol. 22 5, pp. 839–48, 2005.

[22] C. Li, S. Lin, K. Zhou, and K. Ikeuchi, "Radiometric calibration from faces in images," in *Proc. of IEEE Conf. Computer Vision and Pattern Recognition(CVPR)*, 2017, pp. 1695–1704.

[23] H. Li and P. Peers, "Crf-net: Single image radiometric calibration using cnns," in *Proc.of the 14th European Conference on Visual Media Production (CVMP)*, New York, NY, USA, 2017.

[24] S. Mann and R. W. Picard, "Being 'undigital' with digital cameras: extending dynamic range by combining differently exposed pictures," in *Proc. of IS&T*, 1994, pp. 442–448.

[25] M. Grossberg and S. Nayar, "What is the space of camera response functions?" in *Proc. of IEEE Conf. Computer Vision and Pattern Recognition(CVPR)*, vol. 2, 2003, p. 602.

[26] M. Grundmann, C. McClanahan, S. B. Kang, and I. Essa, "Post-processing approach for radiometric self-calibration of video," in *Proc. of IEEE Int. Conf. on Computational Photography(ICCP)*. Cambridge, MA, USA: IEEE, 2013, pp. 1–9.

[27] Y. f. Hsu and S. f. Chang, "Detecting image splicing using geometry invariants and camera characteristics consistency," in *Proc. IEEE Int. Conf. Multimedia and Expo*, Jul. 2006, pp. 549–552.

[28] S. Lin and L. Zhang, "Determining the radiometric response function from a single grayscale image," in *Proc. IEEE Computer Society Conference on Computer Vision and Pattern Recognition CVPR 2005*, vol. 2, 2005, pp. 66–73 vol. 2.

[29] D. Goldman and J.-H. Chen, "Vignette and exposure calibration and compensation," in *Proc. of IEEE Int. Conf. on Computer Vision(ICCV)*, vol. 1. Beijing, China: IEEE, 2005, pp. 899–906.

[30] M. Grossberg and S. Nayar, "Modeling the space of camera response functions," *IEEE Trans. Pattern Anal. Mach. Intell.*, vol. 26, pp. 1272–1282, 2004.

[31] A. Chakrabarti, Y. Xiong, B. Sun, T. Darrell, D. Scharstein, T. Zickler, and K. Saenko, "Modeling radiometric uncertainty for vision with tone-mapped color images," *IEEE Trans. Pattern Anal. Mach. Intell.*, vol. 36, pp. 2185–2198, 2014.

[32] J. Nelder and R. Mead, "A simplex method for function minimization," *Comput. J.*, vol. 7, pp. 308–313, 1965.